

# **Transient Effects in Silicon and InGaAs Avalanche Photodiodes**

**Heidi N. Becker  
Jamie S. Laird**  
Jet Propulsion Laboratory  
California Institute of Technology

**October 31, 2005**

**NEPP FY05 Sensor Technology (Radiation) Task  
NASA UPN: 104-07-01-3  
JPL Project: 102197 JPL Task #3.21.4**

## **1.0 Introduction**

In previous years, this NEPP task has examined the radiation dose response of several classic avalanche photodiodes (APDs) [1]-[4]. In FY05, single event transient (SET) effects from high energy protons, alphas, and heavy ions were studied in these silicon and InGaAs APD technologies. The influence of APD gain on SET amplitudes was of particular interest. APD technologies are attractive for low light applications because of their ability to achieve high internal gain. They are candidate technologies for NASA optical communications and LIDAR applications, in such space environments as Mars and Low Earth Orbit. Protons and low LET ions were used to induce transient events similar to those that might be experienced during solar flares, while in LEO, or in interstellar space.

## **2.0 Samples**

Two silicon APDs were tested: the IR-enhanced C30954E by Perkin Elmer, and the AD-800-9 by Pacific Silicon Sensor. Both silicon devices have a 0.8 mm diameter active area. We also tested the InGaAs C30645E by Perkin Elmer (diameter = 80 microns). The devices are further described in [1]-[4]. The SET test samples were tested in their original metal cans, with the lids removed to avoid attenuating the energy of the incident particles.

## **3.0 Test Methodology**

Separate sets of irradiations were performed using 30-MeV and 63-MeV protons, Po-208, and Cf-252. The proton irradiations were performed at Crocker Nuclear Laboratory, University of California, Davis. Proton fluxes were kept below  $5 \times 10^5$  protons/cm<sup>2</sup> • sec in order to discriminate single-particle SETs and mitigate the number of multiple-particle-induced “pile up” events in the data sets. Accumulated fluences for each sample were kept below  $7 \times 10^8$  protons/cm<sup>2</sup> to minimize dark current increases from displacement damage. The Po-208 and Cf-252 irradiations were performed at the Jet Propulsion Laboratory’s Cf-252 facility. Increases in cumulative damage were also monitored during these experiments.

Figure 3.0.1 shows a diagram of our APD bias circuitry and SET data acquisition system, featuring a charge sensitive pre-amp. The first stage of the SET data acquisition system was the integration of the transient current by an Amptek (A250CF) charge sensitive preamplifier (CSP). The CSP contained an input FET which was thermoelectrically cooled to reduce noise. The input FET was chosen to match the dynamic input capacitance of the APDs. The APD to CSP path-length was also minimized to reduce parasitic capacitance. The gain conversion factor of 4pC/V was set by selecting the appropriate internal feedback capacitor. Finally, the output of the CSP was continuously recorded by a 1GHz bandwidth Tektronix digital storage oscilloscope (DSO) connected via GPIB to a PC running Labview 7.1. A Keithley 237 high voltage bias supply, also controlled with Labview, was used to (a) verify proper current-voltage curves prior to irradiation and (b) provide a programmable high-voltage to set the device bias during irradiation. For a given bias, the trigger level of the DSO was used to window the charge collection spectrum of interest (i.e. in order to separately examine direct and recoil SETs where event rates are at least  $10^5$  times different [5]). Collecting a full spectrum would have resulted in a flood of direct ionization events and at least first-order pileup, which would mask any recoil events. To control noise, cabling was shielded with aluminum foil, and the light-tight chambers used to house the test devices during the Davis and JPL irradiations served as Faraday cages.

Data analysis involved an initial baseline restoration algorithm, which removed any DC offset for each SET. Differentiation was then performed on each SET, and a lower limit threshold was used to remove any false events attributed to noise from surrounding apparatus. Events with multiple edges, such as those generated by event pileup, were also removed. The final reduced pool of events was then calibrated using the above mentioned calibration factors, and the charge height of each SET was used to generate a charge histogram.

A second version of the data acquisition system was used for some data sets. In this implementation the DSO was replaced by an attenuator, amplifier, and MCA. PC-based MCA software was used for collecting SET charge distributions.

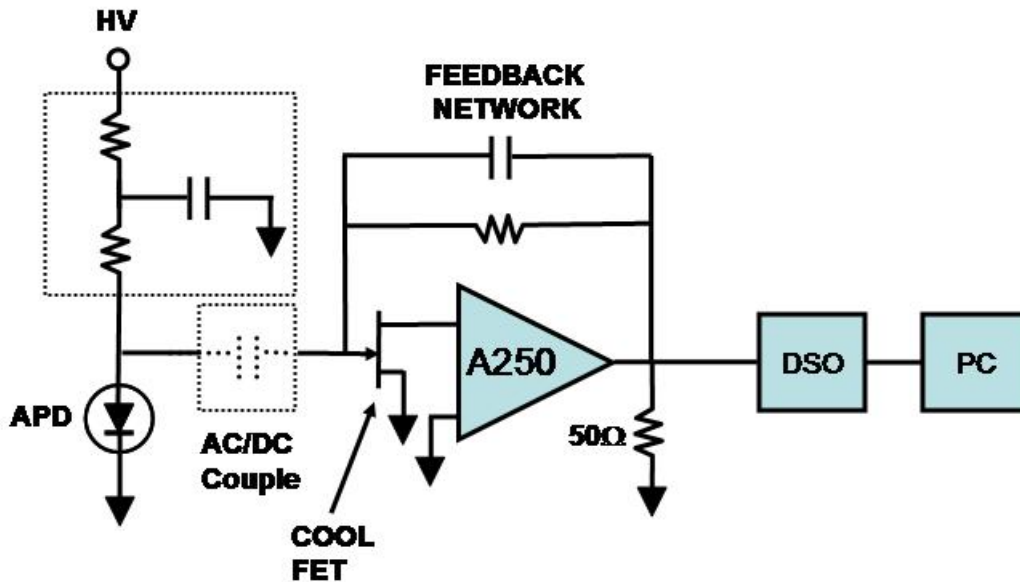


Fig. 3.0.1 SET charge collection apparatus.

SET spectra were collected for each technology under various bias conditions. These biases corresponded to different levels of photon gain ( $M$ ), up to and including the typical linear mode operational gain for each APD technology:  $M = 100$  for silicon and  $M = 10$  for InGaAs. The irradiations were performed at ambient temperature with the test sample in a light-tight chamber. *The entire APD die was exposed to the particle flux.*

## 4.0 Results

### 4.1 Effect of APD Gain on SET Amplitude

The great advantage of APDs in photon-starved applications is their high internal gain (and relatively low noise). To understand the effect of APD gain on SET amplitude, SET charge distributions were examined as a function of APD bias. As expected, the charge distributions were observed to shift as the APD bias was adjusted. However, the gain of the ion-induced signal was significantly less than the corresponding photon gain at typical operational biases.

Fig. 4.1.1 shows SET charge distributions for a silicon Perkin Elmer sample irradiated with 63-MeV protons under two different bias conditions. The scaling has been adjusted to highlight events caused by direct ionization. The sample was irradiated at 200V (which yields a photon gain of ~10 in this technology at 25°C) and at 376V (the voltage required for a photon gain of 100); the peak of the distribution is seen to shift to a higher signal value as the supply voltage is increased.

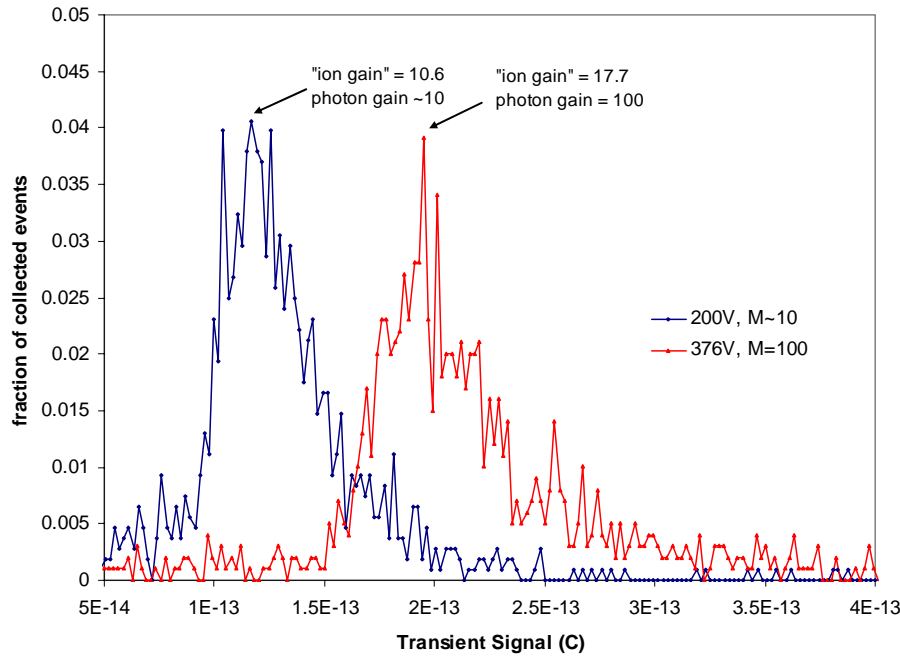


Fig. 4.1.1 Charge distributions for 63-MeV proton-induced SETs in a silicon Perkin Elmer sample. Data were collected at APD photon gains of ~10 (blue) and 100 (red).

The effective amplification factor experienced by the ion-induced signals was analyzed. The most frequently occurring SET value was compared to a calculated signal value based on a simple model for linear energy transfer (LET) in silicon (at normal incidence, assuming no gain):

$$\text{Signal (C)} = \frac{\text{LET} * \rho * t}{E_i} \times q \quad (1)$$

where LET is the linear energy transfer in silicon ( $\text{eV} * \text{cm}^2/\text{g}$ ) for a proton of a given energy,  $\rho$  is the density of silicon ( $\sim 2.3 \text{ g/cm}^3$ ),  $t$  is the thickness of the depletion region (cm), and  $E_i$  is the energy required to create an electron-hole pair in silicon ( $\sim 3.6 \text{ eV}$ ). It is recognized that LET will vary with the

depth of the incident charged particle, and that this will add complexity to the signal profile. This has been demonstrated most recently by Pickel et al. for proton-induced SETs in focal plane arrays [6].

Table 4.1 shows calculated 63-MeV proton-induced signal values for both silicon technologies (assuming no gain). The ratio of the most commonly observed SET signal to the calculated value of deposited charge is used to determine the SET amplification factor, referred to hereafter as “ion gain.” The corresponding gain that would have been experienced by a *photon*-generated signal (at the same supply voltage) is also listed.

**Table 4.1 Observed Amplification Factors for 63-MeV Proton-Induced SETs vs. Photon Gain**

APD Technology	Depletion Region Thickness (cm)	Calculated Signal for 63-MeV proton (assumes no gain) (C)	Most Commonly Observed SET Value (C)	SET Amplification Factor “Ion Gain”	Corresponding Photon Gain for applied supply voltage
Silicon PE*	.013	1.1E-14	1.95E-13	17.7	~100 (376V)
			1.17E-13	10.6	~10 (200V)
Silicon PSS	.006	5.1E-15	4.13E-14	8.1	~50 (200V)
			2.93E-14	5.7	~20 (150V)
			2.29E-14	4.5	~10 (100V)

\*The silicon Perkin Elmer APD was also tested at 30-MeV; a similar trend was observed for both proton energies.

The general trend in Table 4.1 is a *lower amplification factor for ion-induced signals compared to the corresponding photon gain*. In addition, the discrepancy between ion and photon gain increases as the supply voltage is increased. As noted in Fig. 4.1.1, although the ion and photon gains were similar at 200V, the ion gain was only 0.18 times the photon gain at the higher, more typical supply voltage (376V, M=100). SET charge distributions for the Pacific Silicon Sensor APD are shown in Fig. 4.1.2. Bias conditions of 100V (M~10) and 200V (M~50) during 63-MeV proton irradiation are presented. In this device, the ion gain is still less than half the photon gain when M~10.

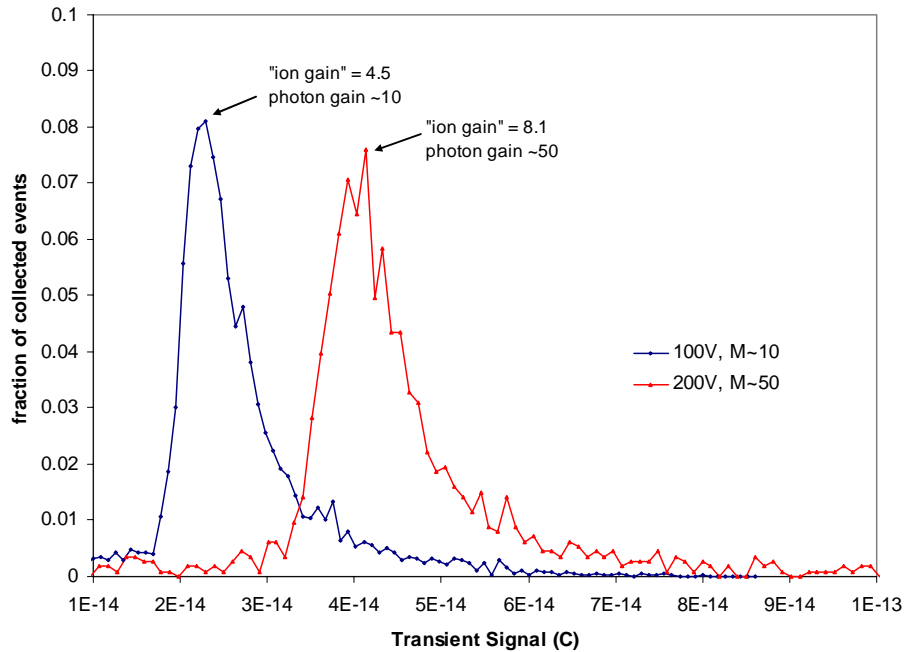


Fig. 4.1.2 Charge distributions for 63-MeV proton-induced SETs in a Pacific Silicon Sensor sample. Data were collected at an APD photon gain of ~10 (blue) and 50 (red).

The lower amplification of ion-induced signal is likely due to space charge screening effects from the ionization charge track in the multiplication region. This can reduce the ensuing amount of impact ionization, and at higher supply voltages (particularly near the “knee” of an APD’s IV curve), the gain is *extremely* sensitive to small changes in the field. It is therefore reasonable to observe a more pronounced screening effect at higher bias. Note that, from a practical standpoint, an APD would typically be operated under a higher supply voltage in order to achieve high photon gain, so the larger discrepancy between ion and photon gain observed at higher bias is probably of most relevance to a space application.

Differences in gain for ion-induced and photon-generated charge are likely due to a range of issues, including but not limited to: (a) space-charge screening effects arising from the relatively dense electron-hole pair track of an MeV ion compared to that of a more diffuse photon source, and (b) markedly different energy-loss profiles for ions and photons of the wavelength used for gain measurements. Photons will generate electron-hole pairs deeper into the absorption region, while ions will generate a more continuous charge track. Carriers need to transit a certain distance to build up an overall gain via impact ionization. Much of the ion-generated charge will not have this opportunity.

Every APD will have a somewhat unique field profile, dependent on its structure, and this could lead to differences in SET amplitudes even among technologies with similar depletion thicknesses. For instance, the most frequently observed 63-MeV proton SET in the silicon Perkin Elmer APD was five times larger than that of the Pacific Silicon Sensor device (for  $M \sim 10$ ). The Perkin Elmer depletion region is twice as thick as that of the PSS device, which is one contributor to the difference in transient amplitude. The additional factor of 2.5 may be due to other structural differences that influence the size and location of the fields in the two devices.

## **4.2 Comparison of 30-MeV and 63-MeV Proton-Induced SET Spectra**

SET charge spectra for the silicon Perkin Elmer APD were taken using both 30- and 63-MeV protons. The signal values corresponding to the peaks of the distributions were compared. The most frequently observed 30-MeV SET was approximately 1.5 times higher than those observed with 63-MeV protons. This was true for both  $M=10$  and  $M=100$ , and is also in very good agreement with the 1.78 difference in stopping powers (LET) for 30- and 63-MeV protons in silicon [7]. Figure 4.2.1 shows spectra for both operational conditions for 30-MeV and 63-MeV protons ( $M \sim 10$  for blue distributions, and  $M=100$  for red distributions).

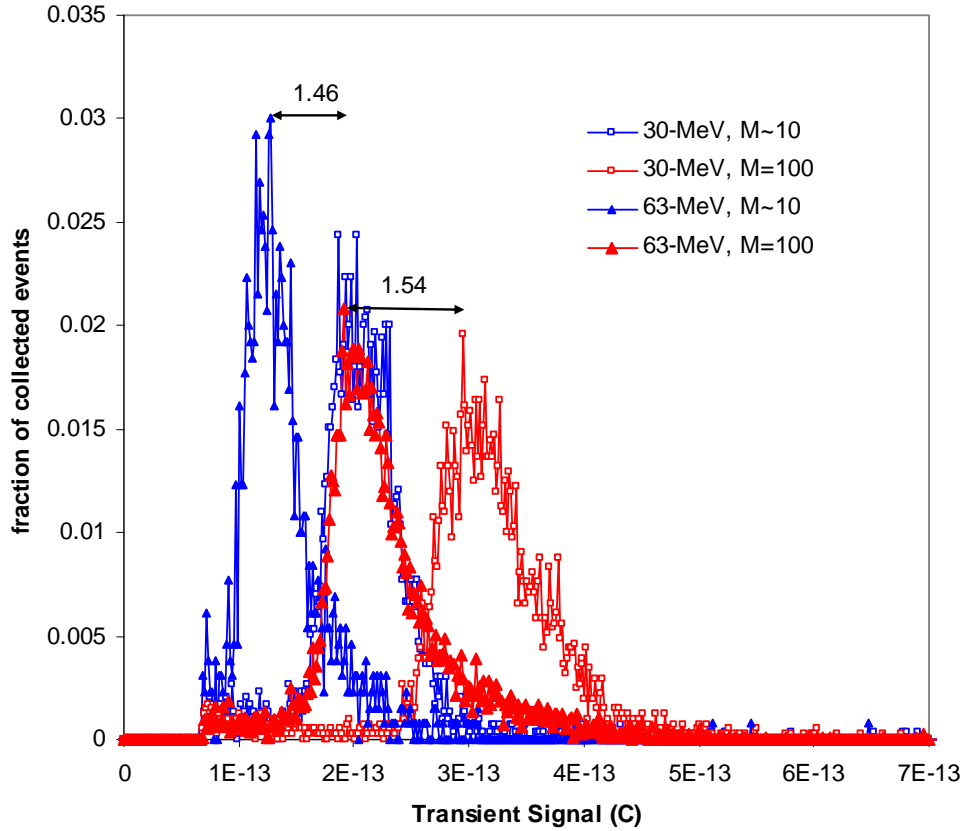


Fig. 4.2.1 SET charge distributions for the silicon Perkin Elmer APD. Distributions for 30-MeV and 63-MeV protons are compared at biases corresponding to photon gains of  $\sim 10$  and 100.

### 4.3 Comparison of SET Amplitudes for InGaAs and Si APDs

The typical signal size of SETs in the Perkin Elmer InGaAs APD was about an order of magnitude smaller than those observed for the two silicon APDs. This was expected, since the depletion region of the InGaAs technology is only a few microns thick, while the silicon devices have 60-130 micron thicknesses. Fig. 4.3.1 shows 63-MeV proton SET charge distributions for the InGaAs APD at 40V and 47V. As with the silicon technologies, the ion gain did not match the photon gain for a given bias condition. Note that the distributions in Fig. 4.3.1 are essentially the same, despite the factor of 2 difference in photon gain for these two supply voltages.

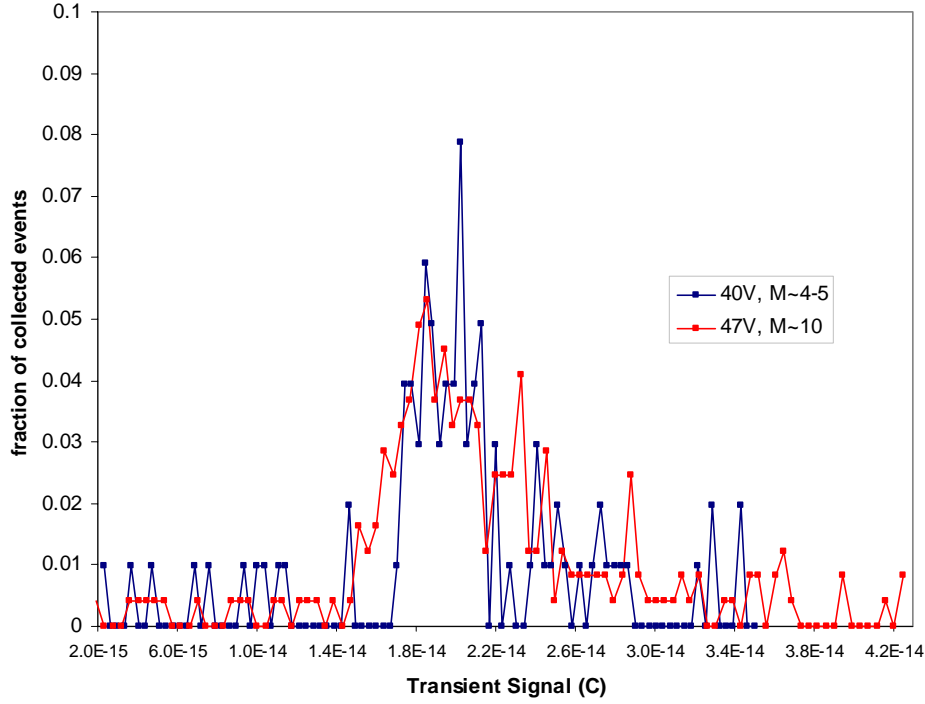


Fig. 4.3.1 SET charge distributions for the InGaAs Perkin Elmer APD. The device was irradiated with 63-MeV protons at biases corresponding to photon gains of 10 and ~4-5.

The impact of a 20 fC SET would depend on the tolerances of the particular application. Recoils will cause larger SETs, but may be easier to discriminate in a photon-starved application where more subtle signal levels are important (as in a LIDAR mapper). In addition, recoil events are much less numerous than SETs from direct ionization. Johnston et al. observed a ratio of  $\sim 10^5$  direct ionization events for each recoil event in a 50 micron surface barrier detector using 40-MeV protons [5].

#### 4.4 Species Comparisons

Our proton-induced SET charge distributions were compared to spectra taken using a 5-MeV alpha source (Po-208), and Cf-252 decay products. As with our proton data, a space charge screening effect appeared to influence the degree of SET amplification. Further, using particles with a higher track density (LET) seems to increase this effect, because only very small increases in ion gain were observed as the supply voltage was increased over 200V (for the silicon APD).

The 5.11-MeV alphas from Po-208 are stopped before passing through the 130 micron depletion region of the silicon Perkin Elmer APD, so a signal on the order of 100 fC would be expected with no amplification. We saw two peaks in the Po-208 charge distributions for this APD. One was at  $\sim 200$  fC, and the other was near 1 pC. The lower peak may be due to the 0.571 and 0.603 MeV gamma emissions of Po-208. Figure 4.4.1 shows the Po-208 charge distribution for a silicon Perkin Elmer sample, and Fig. 4.4.2 highlights the second peak in the distribution. The supply voltages represented here range from that required for a photon gain of  $<10$  (150V) to above the breakdown voltage of this sample (350V). The broadening of the peak at 350V may be related to field effects as the device goes into breakdown. However, there is very little difference in signal amplification for this range of voltages. The amplification factor is essentially 10 for all cases.

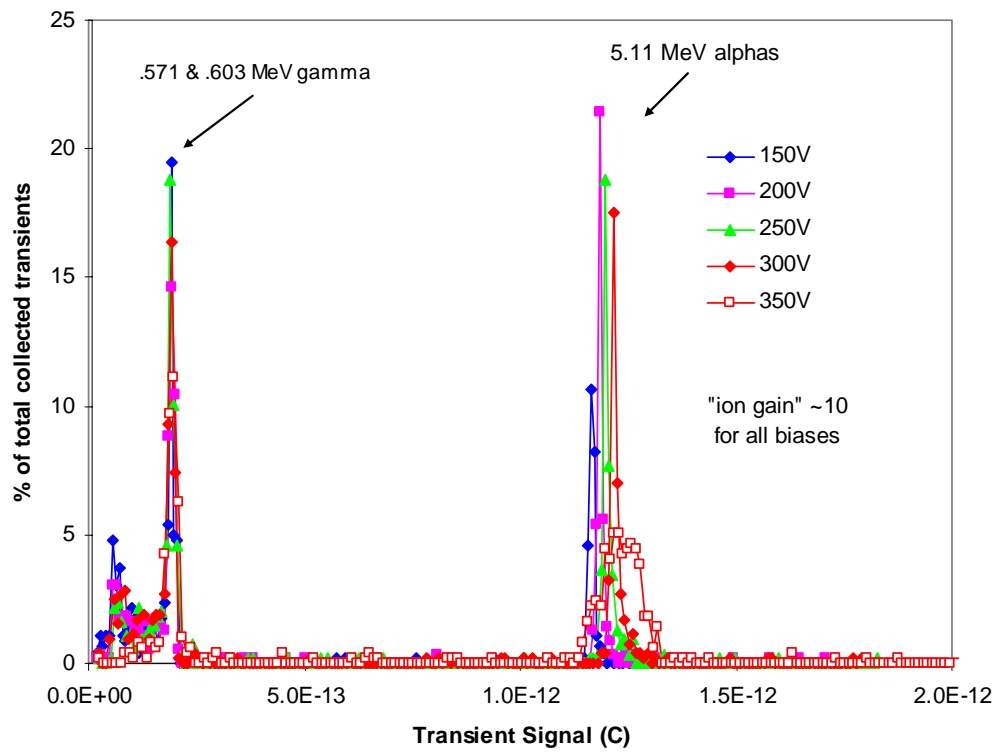


Fig. 4.4.1 Po-208 charge distributions for the silicon Perkin Elmer APD.

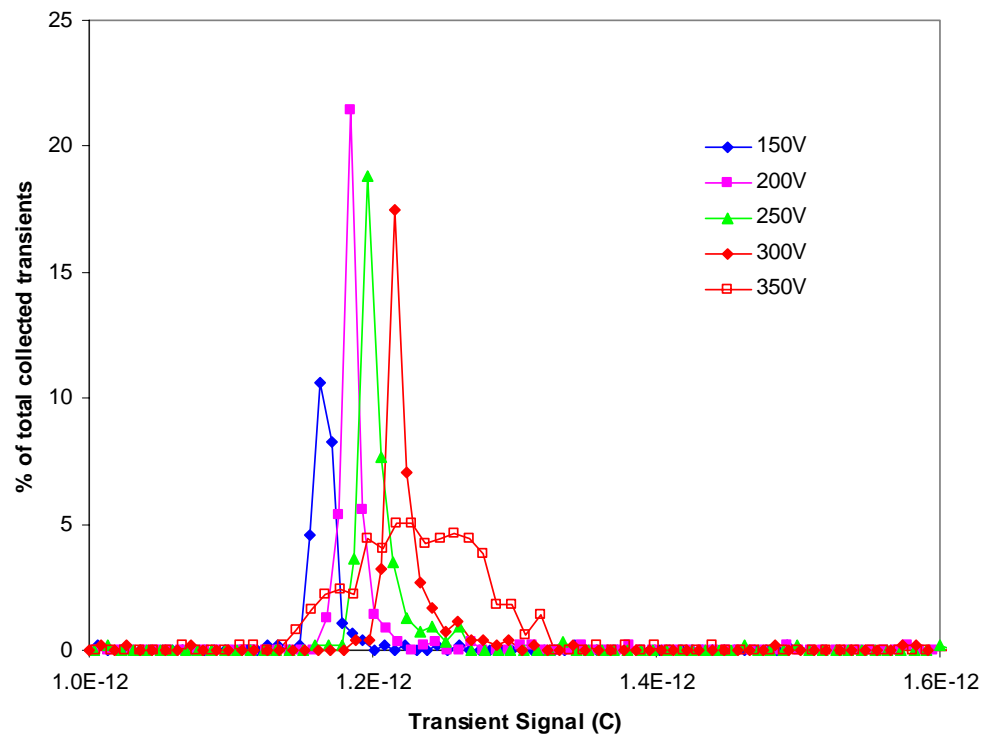


Fig. 4.4.2 The second peak of the Po-208 charge distribution for the silicon Perkin Elmer APD.

The InGaAs Perkin Elmer APD was also irradiated with Po-208 (see Fig. 4.4.3). The peak of its distribution is near 100 fC. This is ten times lower than for the silicon device, which is consistent with the trend observed in our proton data for these two materials. 30V corresponds to a photon gain of ~1 (it is just above the punch through voltage), and 47 V yields a photon gain of 10.

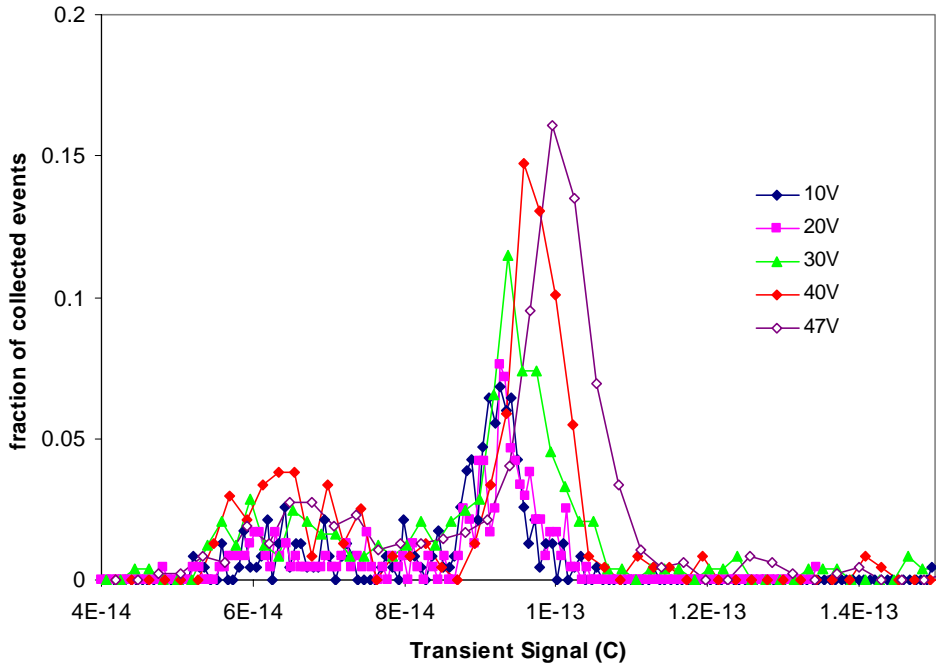


Fig. 4.4.3 Po-208 charge distributions for the InGaAs APD.

The InGaAs APD was also irradiated with Cf-252 (the SET signals that were generated in the silicon devices with Cf-252 saturated our charge sensitive pre-amp so the silicon APDs were not characterized with that source). We were able to collect SET values up to 2 pC, but it is believed that the majority of the SETs from the heavy ion decay products occur above this rail. The peak observed in Figure 4.4.4 is believed to be coming from the 6-MeV alpha product that is part of the rather complex cocktail of products emitted by the Cf-252 source. Considering the trend observed in our proton and alpha data, it is expected that ion gain would remain low at high biases for particles with larger track densities. Further testing or modeling would be required to determine this.

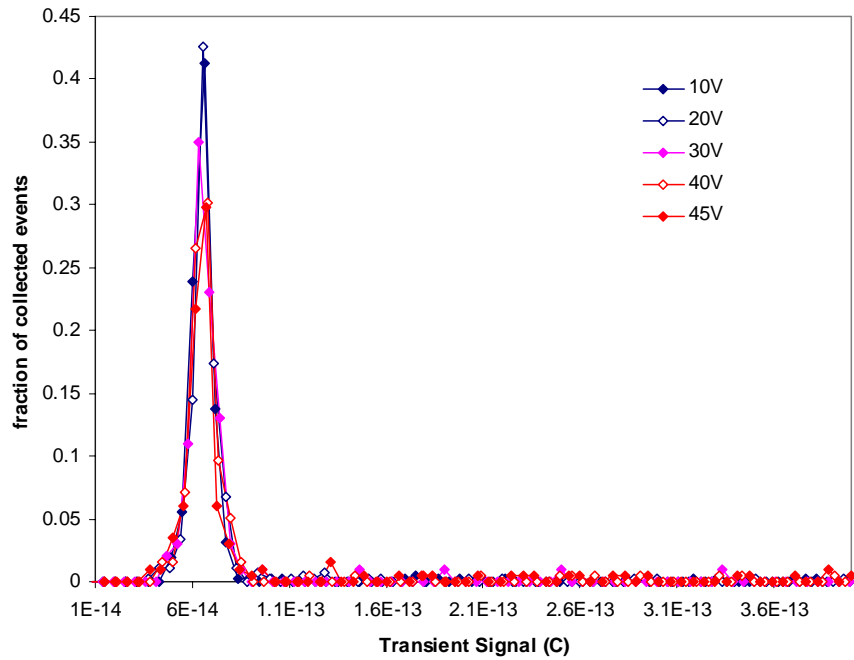


Fig. 4.4.4 Cf-252 charge distributions for the InGaAs APD.

## 5. Conclusions

Single event transient testing of silicon and InGaAs avalanche photodiodes has shown lower amplification factors for ion-induced signals, compared to photon-generated signals, for a given bias condition. This is likely due to space charge screening effects in the multiplication region. The amount of field screening appears to be affected by the applied potential across the junction and the LET of the incident particle. SETs from particles of higher LET were seen to be less sensitive to internal APD gain.

It is proposed that structural differences among APDs, beyond depletion thicknesses, can influence the field profiles and thus the amount of SET amplification. The impact of an SET of a given amplitude is highly dependent on the application in question. Photon-starved applications are more likely to be disrupted by lower signal SETs. It would be interesting to extend this study to determine SET amplitudes for classic APDs operated in Geiger mode (above the breakdown voltage).

## 6. Acknowledgements

We would like to thank Tetsuo Miyahira of the Jet Propulsion Lab for assistance with the irradiations. This research was carried out at the Jet Propulsion Laboratory, California Institute of Technology, under a contract with the National Aeronautics and Space Administration as part of the NASA Electronic Parts and Packaging Program, Code Q. Reference herein to any specific commercial product, process, or service by trade name, trademark, manufacturer, or otherwise, does not constitute or imply its endorsement by the United States Government or the Jet Propulsion Laboratory, California Institute of Technology.

## 7. **References**

- [1] H.N. Becker, “FY04 NEPP TRO – Sensor Technology: Near Infrared Avalanche Photodiodes,” October, 2004.
- [2] H.N. Becker and A.H. Johnston, “Dark current degradation of near infrared avalanche photodiodes from proton irradiation,” *IEEE Trans. Nucl. Sci.*, vol. 51, no. 6, pp. 3572-3578, Dec. 2004.
- [3] H.N. Becker, T.F. Miyahira, and A.H. Johnston, “The Influence of Structural Characteristics on the Response of Silicon Avalanche Photodiodes to Proton Irradiation,” *IEEE Trans. Nucl. Sci.*, vol. 50, no. 6, pp. 1974-1981, Dec. 2003.
- [4] H.N. Becker, “FY03 NEPP TRO – Improved Radiation Qualification & Test Methods: Optical Detector Noise Characterization (Avalanche Photodiodes),” September, 2003.
- [5] A.H. Johnston, et. al, “Angular and Energy Dependence of Proton Upset in Optocouplers,” *IEEE Trans. Nucl. Sci.*, vol. 46, no. 6, pp. 1335-1341, Dec. 1999.
- [6] J.C. Pickel et al., “Transient Radiation Effects in Ultra-low Noise HgCdTe Detector Arrays for Space-based Astronomy,” *IEEE Trans. Nucl. Sci.*, to be published Dec. 2005.
- [7] NIST PSTAR, <http://physics.nist.gov/PhysRefData/Star/Text/PSTAR.html>, August, 30, 2005.